Computational Materials Science 50 (2011) 1731–1743

Contents lists available at ScienceDirect

Computational Materials Science

journal homepage: www.elsevier.com/locate/commatsci

Stability and size-dependency of temperature-related Cauchy–Born hypothesis

A.R. Khoei *, P. Ghahremani, M.J. Abdolhosseini Qomi, P. Banihashemi

Center of Excellence in Structures and Earthquake Engineering, Department of Civil Engineering, Sharif University of Technology, P.O. Box. 11365-9313, Tehran, Iran

ARTICLE INFO

Article history:
Received 5 August 2010
Received in revised form 27 December 2010
Accepted 7 January 2011
Available online 3 February 2011

Keywords:
Temperature-related Cauchy–Born
Size effect
Molecular dynamics
Nose–Hoover thermostat

ABSTRACT

In continuum mechanics, the constitutive models are usually based on the Cauchy–Born (CB) hypothesis which seeks the intrinsic characteristics of the material via the atomistic information and it is valid in small deformation. The main purpose of this paper is to investigate the temperature effect on the stability and size-dependency of Cauchy–Born hypothesis. Three-dimensional temperature-related Cauchy–Born formulations are developed for crystalline structure and the stability and size-dependency of temperature-related Cauchy–Born hypothesis are investigated by means of direct comparison between atomistic and continuous mediums. In order to control the temperature effect, the Nose–Hoover thermostat is employed. Since the Helmholtz free energy is temperature dependent; the first Piola–Kirchhoff stresses are explicitly computed as the first derivative of the Helmholtz free energy density to the deformation gradient. It is numerically shown that the validity surfaces become smaller at higher temperature, which is significant in larger specimen. It is also presented that the material stability decreases with increasing the ambient temperature.

1. Introduction

Continuum models are expected to cover small deformation in large nano-scale simulation, as an alternative for molecular dynamics (MD) since they are feasible for expensive simulation. Physical phenomena in real world are attracted by temperature effects and its thermodynamics. Most available continuum models are assumed at zero temperature, so the calculated stress is only valid for the potential part of energy, such an assumption could not exactly present the temperature-related physical phenomena. Therefore it is important to implement the temperature effects in continuum model when performing simulation. Furthermore, the material instability is always attractive to scientists and researcher of material science and continuum mechanics, since the failure criteria have been generally changed by the temperature.

The Cauchy–Born hypothesis employs the homogenization theory and seeks intrinsic characteristics of material via the atomic information that is applied in continuum models. In this theory, it is assumed that the deformations are quite small. When the solid state materials are subjected to small loading, the crystalline lattice is stable; thus the CB is valid until solid to solid phase transformation occurs. All crystalline material shows this transformation and this unstable condition affected specially by thermo-mechanical load. The CB hypothesis is generally assumed at zero temperature, which does not show the ability to model the temperature effect in physical incident.

The validity of Cauchy–Born hypothesis has been investigated by various researchers. A stability criterion was presented by Wang et al. [1], which was not able to model the crystalline instability in uniaxial tension on thermal loading. Braides [2] studied the atomistic model using the concept of Γ-convergence and proved that the certain discrete function with pair-wise interaction converges to a continuum model. Klein and Gao [3] and Zhang et al. [4] established an approach to combine the atomistic model with the continuum analysis. Friesecke and Theil [5] proposed a 2D-cubic lattice model with harmonic springs between the nearest and diagonal neighbors to mathematically inquire into the validity of CB hypothesis. Friesecke and James [6] introduced an atomic model into the continuum theory for two-dimensional structures such as thin films and nanotubes. Arroyo and Belytschko [7], Zhang et al. [8] and Jiang et al. [9] proposed the nano-scale continuum theories for carbon nanotubes based on the interatomic potentials for carbons. Khoei et al. [10] and Aghaei et al. [11] introduced two failure criteria in the strain and stress domains to acquire the validity curves for 2D and 3D F.C.C. lattices. The resultant curves for CB hypothesis were similar to those of yield surfaces obtained in continuum mechanics and plasticity. Recently, the boundary Cauchy–Born technique was developed by Abdolhosseini et al. [12] for multiscale modeling of surface effect in crystalline nanostructures. The above theories were based on molecular dynamics or often atomistic simulation; however they are limited to zero temperature and do not accounted for the effect of temperature.

The effect of temperature can be accounted via the local harmonic approximation relating the entropy to the vibration frequencies of the system. The instant temperature in molecular

* Corresponding author. Tel.: +98 (21) 6600 5818; fax: +98 (21) 6601 4828.
E-mail address: arkhoei@sharif.edu (A.R. Khoei).

0927-0256/$ - see front matter © 2011 Elsevier B.V. All rights reserved.
doi:10.1016/j.commatsci.2011.01.004

dynamic simulation is defined by the summation of kinetic energy over all degrees of freedom divided by the number of degrees of freedom. Jiang et al. [13] established a finite temperature continuum theory directly from the interatomic potentials and studied several temperature-related material properties based on the Brenner's interatomic potential [14] and its second generation potential for carbon. Xiao and Yang [15] and Yun and Park [16] developed a temperature-related Cauchy–Born rule for multiscale modeling of crystalline solids. Yang and Xiao [17] studied the material stability of nanostructure material via the continuum linearized stability analysis with TCB rule and shown that the nanostructure materials are more stable at lower temperatures. They also shown that at the same temperature, stiff materials could sustain larger deformation than soft materials. However, they did not perform direct comparison between molecular dynamic and continuum models to obtain the exact failure criterion between two models. Aghaei et al. [11] studied the size-dependency and the validity of CB hypothesis in 3D lattice structures, however, they did not take the temperature effects into account.

In the present paper, the temperature effects and the validity of temperature-related Cauchy–Born hypothesis are presented in three-dimensional lattice structures by comparatively analyzing results of the continuum mechanics calculation and molecular dynamics simulations. In order to consider the real metallic behavior in numerical simulations, the Sutton–Chen many-body potential is employed. In MD simulation, the Nose–Hoover thermostat is applied to control the temperature and perform simulation at constant temperature. In modeling of crystalline solids, the deformation is assumed to be homogeneous and atoms have the same local vibration mode, while the coupled vibration of different atoms is negligible. In temperature related studies of material behaviors at nano-scale, the resultant curves indicate a strong correlation between the material stability and thermal conditions.

2. Temperature-related Cauchy–Born hypothesis

The temperature-related Cauchy–Born hypothesis is a hierarchical assumption for modeling elastic behavior of material due to temperature effect. The physical phenomena at nano-scale, particularly the failure of nanostructure material, are temperature related. In this study, the Helmholtz free energy is considered instead of the potential energy, in which the atoms at finite temperature occupy new positions due to thermal vibrations. The Helmholtz free energy $W_H = W_C - TS$ depends on the atomic bond length r, temperature T, and the entropy S. The entropy S in Helmholtz free energy can be calculated from quasiharmonic approximation expressed for the system of size N as

$$S = -k_B \sum_{n=1}^{3N} \ln\left[2\sinh\left(\frac{hw_n}{4\pi k_B T}\right)\right] \tag{1}$$

The vibration of atom in a crystalline solid is assumed to be harmonic, so the Helmholtz free energy W_H of a crystalline solid, which contains N atoms at temperature T, is given by [18]

$$W_H = W_c(x) + k_B T \sum_j \ln\left[2\sinh\left(\frac{hw_j}{4\pi k_B T}\right)\right] \tag{2}$$

where $W_c(x)$ is the potential energy of atoms in their equilibrium at position x at zero temperature, h is the Planck's constant and k_B is the Boltzmann constant. The sum over j includes all the non-zero vibrational modes of the system. The frequencies w_j are the Eigen values of dynamical matrix

$$D_{I\alpha J\beta} = \frac{1}{\sqrt{m_I m_J}}\left(\frac{\partial^2 w_0}{\partial X_{I\alpha}\partial X_{J\beta}}\right) \tag{3}$$

where $X_{I\alpha}$ is the vibrational coordinate in direction α for atom I, and m_I is the mass of atom I. Eq. (2) can be simplified as

$$W_H = W_c(x) + nk_B T \sum_{I=1}^{N} \ln\left[\left(\frac{h\overline{D}_I^{\frac{1}{2n}}}{2\pi k_B T}\right)\right] \tag{4}$$

where $\overline{D}$ is the determinant of local dynamical matrix.

The Sutton–Chen many-body potential is chosen here for the calculation of potential energy defined as [19]

$$w_0 = w_{0i} = \frac{\varepsilon}{\Omega_{0i}}\left[\frac{1}{2}\sum_{j\neq 1}\left(v(r_{ij}) - c\sqrt{\rho_i}\right)\right] \tag{5}$$

where $v(r_{ij}) = (a/r_{ij})^n$ and $\rho_i = \sum_{i\neq j}(a/r_{ij})^m$. In above relation, Ω_{0i} is the local atomic volume in relaxed and undeformed configuration of the lattice structure associated with atom i, w_{0i} is the potential

Table 1
The effect of total simulation time and the number of time steps on the size of specimen for the 4000 atoms specimen at 400 °K.

Total simulation time (picoseconds)	Number of time steps	Size of cube in x-direction	Size of cube in y-direction	Size of cube in z-direction
160	320,000	9.98	10.01	9.87
240	480,000	9.98	9.95	9.96
320	640,000	10.02	9.99	9.91
480	960,000	9.94	9.93	10.04

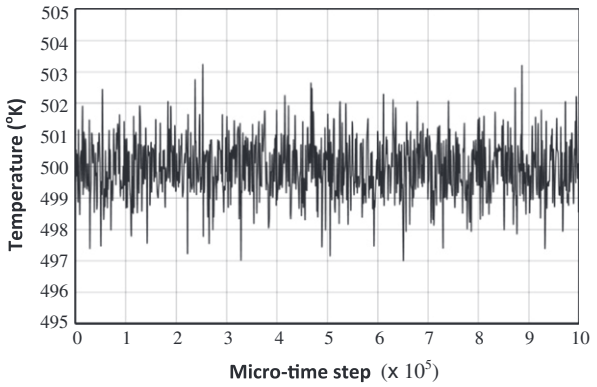

Fig. 1. The variation of temperature with micro-time steps after relaxation phase for 4000 atoms specimen at 500 °K.

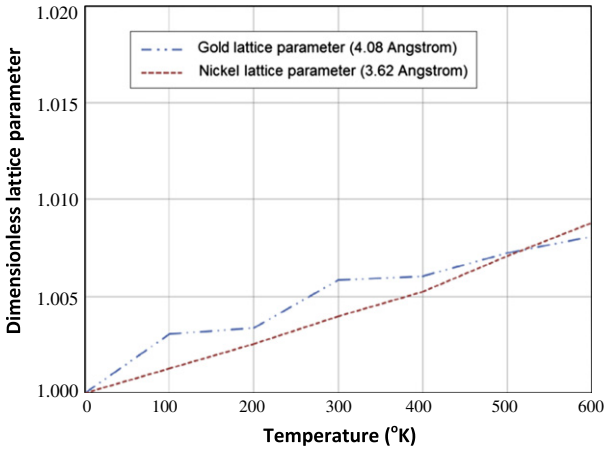

Fig. 2. Comparison of the lattice parameter derived by Dupuy et al. [23] and that obtained by present model for Nickel with 1372 atoms specimen (all values are divided to its material lattice parameter at 0 °K to make the value dimensionless, and the numbers in parentheses show the material lattice parameter at 0 °K).

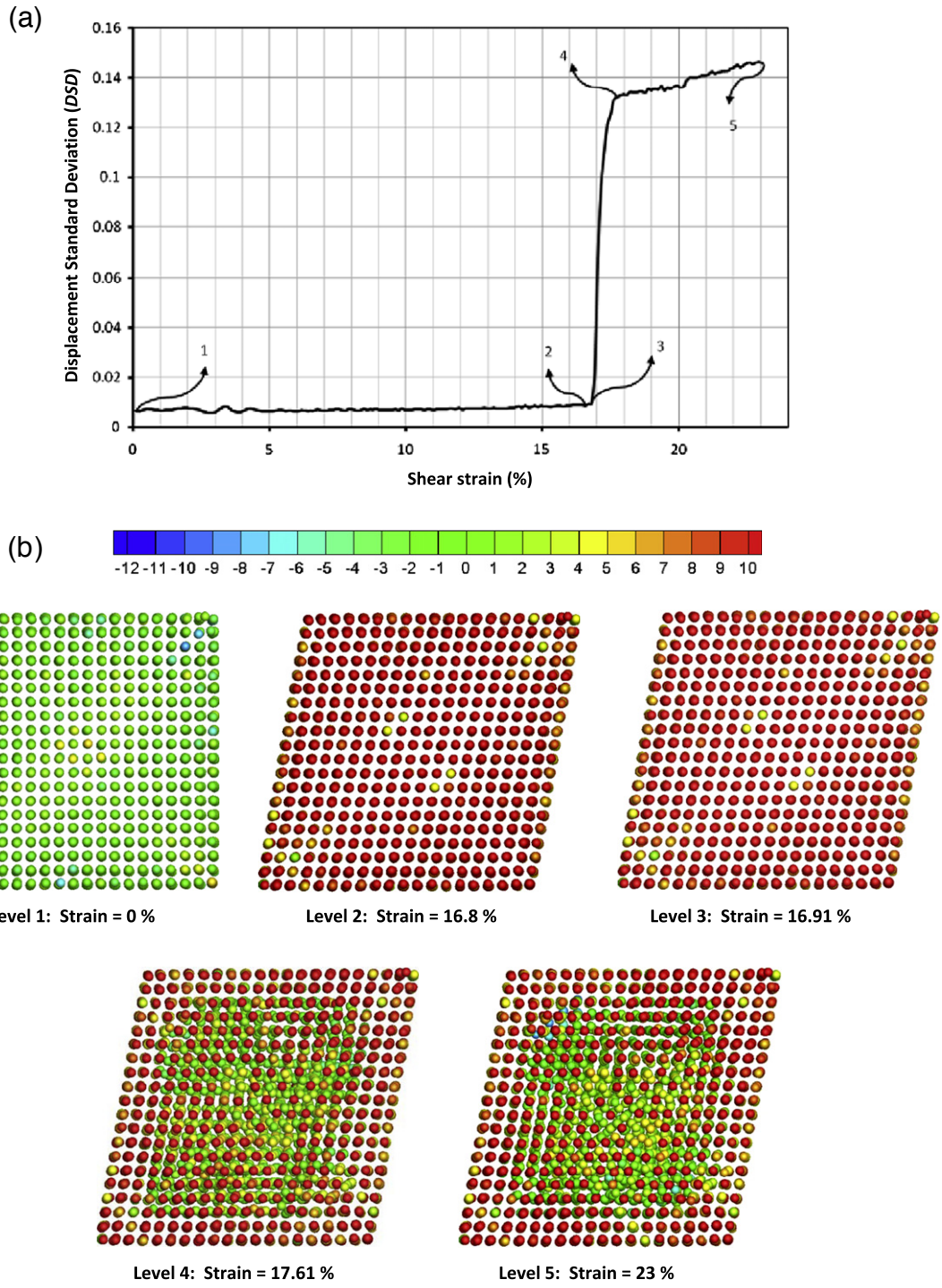

Fig. 3. (a) The variation of DSD with shear strain for 4000 atoms specimen at 100 °K, (b) the evolution of atomic positions during the simulation; the thermal CB model fails at the third level.

energy of atom i, r_{ij} is the inter atomic distance between the host and its neighbor j, a is the lattice parameter and m, n, c and ε are the potential parameters. These constants are obtained for ten different materials by Sutton and Chen [19].

In hyperelasticity, the stress tensor is derived by differentiating the strain energy density of deformed material with respect to the deformation gradient. Hence, the first Piola–Kirchhoff stress tensor P_{ij} can be calculated as the first derivative of free energy density W_H, which is a function of temperature and deformation gradient as

$$P_{ij}(\mathbf{F},T)=\frac{\partial W_H(\mathbf{F},T)}{\partial F_{ij}} \tag{6}$$

in which the above definition is derived for three-dimensional lattice structure as

$$\mathbf{P}=\frac{\partial W_c}{\partial \mathbf{F}^T}+\frac{K_B T}{\sqrt{3\overline{D}}r_0^2}\frac{\partial \overline{D}}{\partial \mathbf{F}^T} \tag{7}$$

where $\mathbf{F}$ is the deformation gradient and r_0 is the initial distance between atoms.

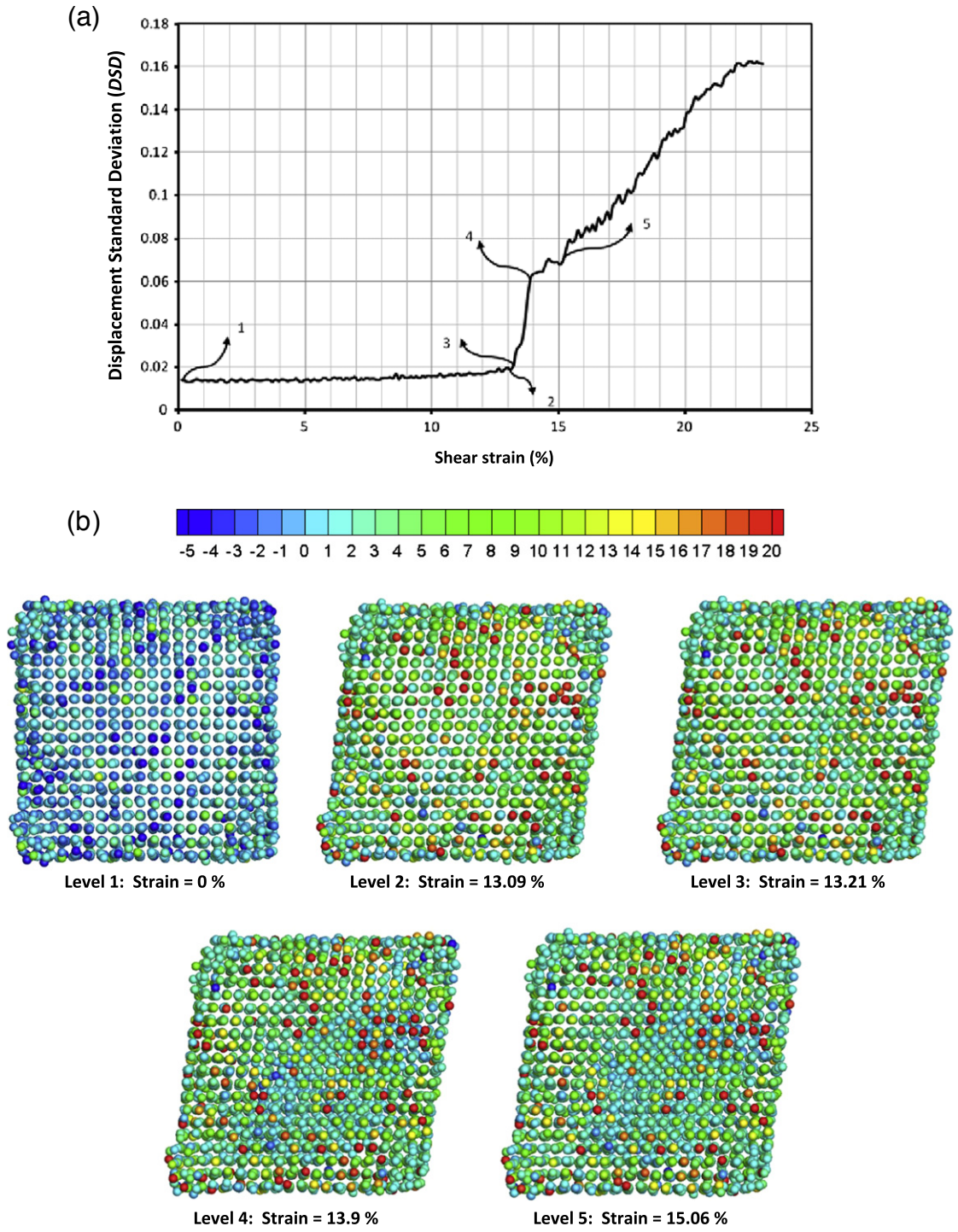

Fig. 4. (a) The variation of DSD with shear strain for 4000 atoms specimen at 500 °K, (b) the evolution of atomic positions during the simulation; the thermal CB model fails at the third level.

3. Molecular dynamics modeling

The MD simulation is a powerful technique for computing the equilibrium and non-equilibrium characteristics of materials. The method is used to determine the validity and failure of the TCB hypothesis. The MD method is a numerical solution of second Newton law of motion in time domain. The finite difference method for solving differential equations is based on the Velocity-Verlet algorithm proposed by Allen and Tildesley [20]. The force acting on the *i*th particle is calculated using the Sutton–Chen many-body potential (Eq. (5)). The MD equations are solved by the assumptions of constant temperature, volume and number of atoms. In the MD simulation, the temperature control is critical as most experimental measurements are executed at constant temperature rather than constant energy. Here, the Nose–Hoover method thermostat is implemented to control the temperature [21]. The method resolves the temperature control difficulty by deriving the dynamics from an extended Hamiltonian that can be shown to give canonically distributed positions and momentum. The Nose–Hoover is based on the following assumptions; the dynamics

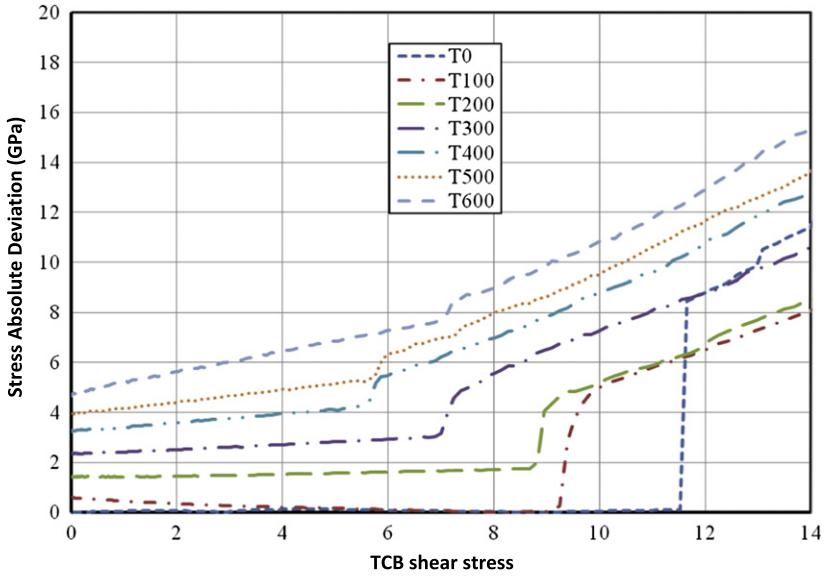

Fig. 5. Simple shear deformation; the evolution of SAD shear component versus TCB shear stress at various temperatures for 4000 atoms specimen.

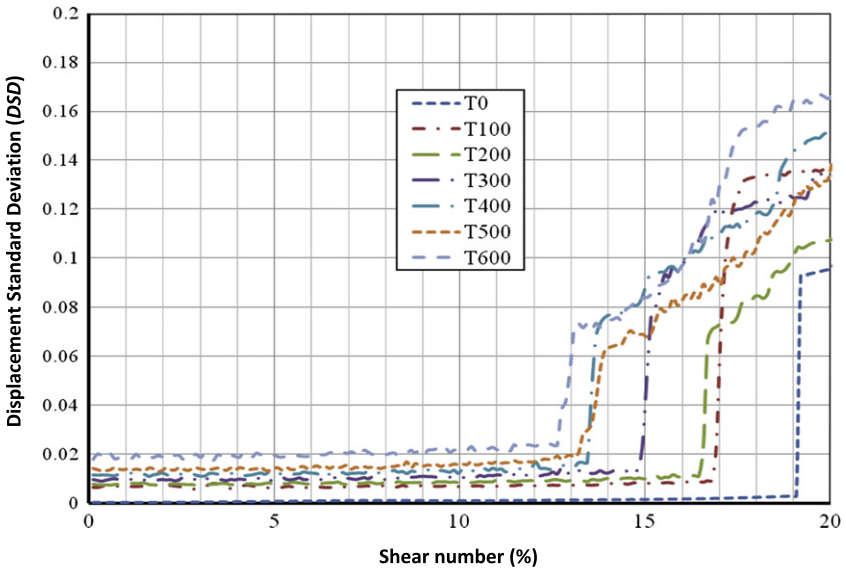

Fig. 6. Simple shear deformation; the evolution of DSD shear component versus shear number at various temperatures for 4000 atoms specimen.

is ergodic and the experimental systems are large so this algorithm could generate the correct distribution in constant temperature. Assume that the NVT system is a part of large NVE structure. The Hamiltonian of system can be written as

$$H = \sum \frac{1}{2} S^2 r_i^2 \underline{r}_i^2 + V(r^N) + \frac{Q}{2}\underline{S}^2 + \frac{g}{\beta} \ln S \tag{8}$$

In this thermostat, the parameters Q and S are inserted to control the temperature of system. If Q increases, the friction between atoms increases and at low temperature, the large value of Q freezes the atom structure.

The validity of TCB can be investigated by computing the deformation of the continuous and atomistic mediums. The elastic modulus can be used for the assessment of validity of the TCB hypothesis. Since the strains must be applied at the boundaries of atomic model, and the continuum specimens are identical, various stress measurements have been defined by researchers to evaluate the atomic stress. Subramanian and Sun [22] have shown that for those simulations carried out at zero temperature, the Virial stress, BDT stress and Cauchy stress are identical. In order to implement the temperature effects on atomic stress, the kinematic part of stress is calculated. The BDT stress has similar stress in a homogenously deformed system. A small perturbation in the atomic configuration will change atomic stresses. Thus, it is important to use the average stress for atomic scale which represents the continuum mechanics stress at continuum points as

$$\sigma_{\mathrm{MD}}^{\alpha\beta} = \frac{1}{N}\sum_{i=1}^{N} \sigma_i^{\alpha\beta} \tag{9}$$

where N is the total number of unconstrained atoms, $\sigma_{\mathrm{MD}}^{\alpha\beta}$ is the $\alpha\beta$th component of the average BDT stress tensor derived by the MD simulation.

Two distinct failure criteria are used in the strain and stress domains to check the validity of TCB hypothesis. Applying a uniform deformation at the boundary atoms, the remaining internal atoms

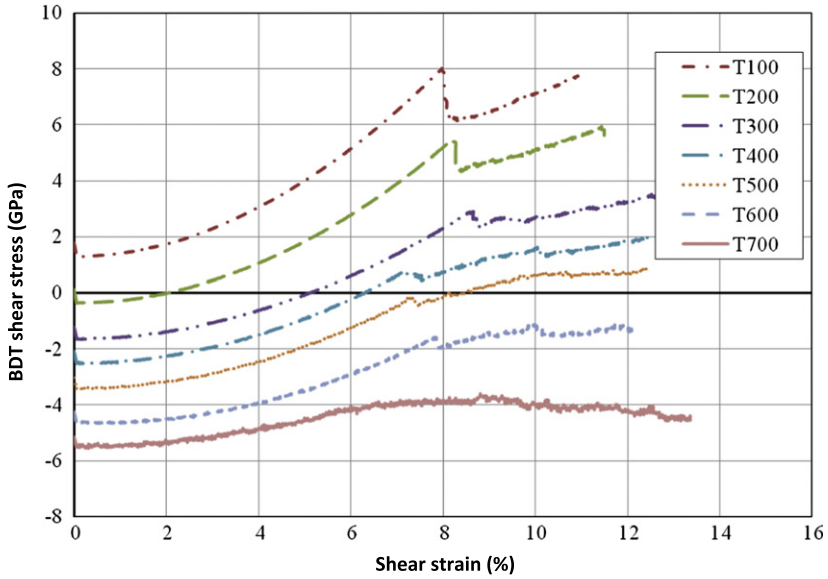

Fig. 7. Simple shear deformation; the variations of BDT shear stress with shear strain at various temperatures for 4000 atoms specimen.

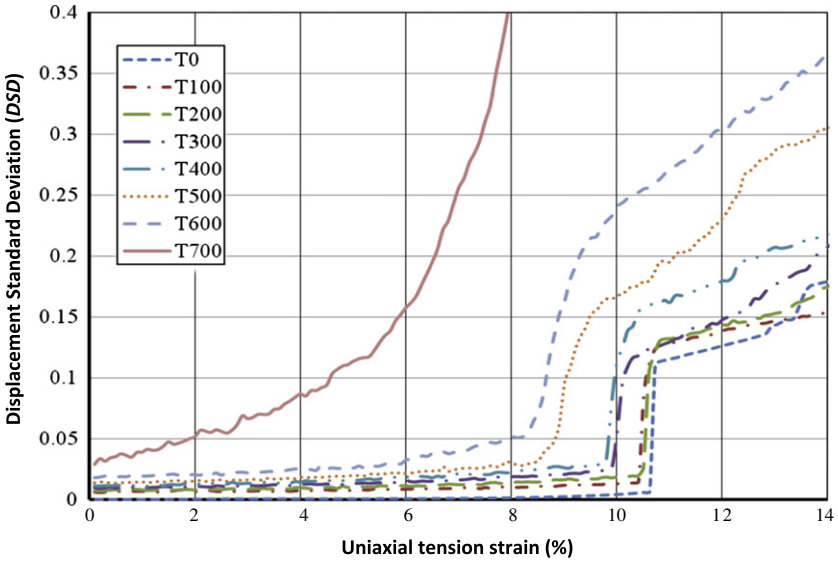

Fig. 8. Uniaxial deformation, the evolution of DSD versus uniaxial tension strain at various temperatures for 8788 atoms specimen.

are set free to direct the system to its local minimum energy in specific temperature. The configuration of MD simulation is not equal to the deformation predicted by TCB. The displacement standard deviation DSD is derived as

$$\mathrm{DSD} = \frac{1}{a}\sqrt{\frac{1}{3N-1}\sum_{i=1}^{N}(r_i^{\mathrm{MD}} - r_i^{\mathrm{CB}})^2} \tag{10}$$

where N is the total number of particles, and r_i^{MD} and r_i^{CB} are the spatial coordinate vectors of ith atom computed by means of MD solution and TCB hypothesis. The validity of TCB in strain domain is calculated by this formula. The stress absolute deviation from the temperature-related Cauchy–Born hypothesis is defined as

$$\mathrm{SAD}^{\alpha\beta} = |\sigma_{\mathrm{MD}}^{\alpha\beta} - \sigma_{\mathrm{CB}}^{\alpha\beta}| \tag{11}$$

where $\sigma_{\mathrm{CB}}^{\alpha\beta}$ is the component of Cauchy stress tensor calculated by means of the TCB hypothesis.

4. Numerical simulation results

In order to evaluate the limitation of TCB hypothesis in 3D applications, several MD simulations have been carried out at various temperatures with different sizes and deformation paths. The effect of temperature is investigated and the validity surface is achieved for the Gold metal by applying several triaxial deformation paths at different temperatures and various sizes for cubic specimens. In order to perform the numerical simulation, four single crystalline cubic specimens are produced in conformity with the ideal geometrical F.C.C. lattices. These samples are chosen with the size of 1372, 4000, 8788 and 16,384 Gold atoms and temperatures vary from 0 to 700 °K. Since the temperature has a significant influence in numerical results, which produces fluctuation in the system, the effect of temperature is important on the surface of specimen. Furthermore, because of the high ratio of the surface to volume in 3D nano-scale specimens, the size effect has a significant effect on thermal results.

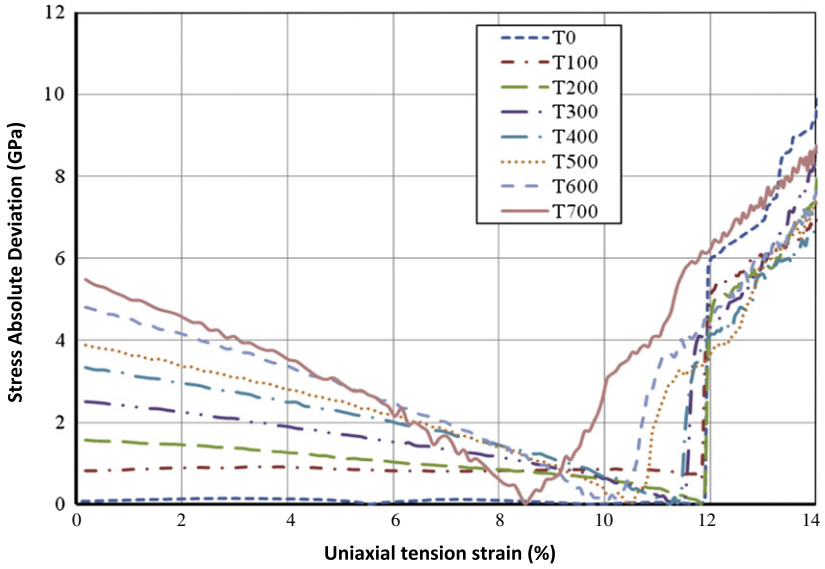

Fig. 9. Uniaxial deformation, the evolution of SAD versus uniaxial tension strain at various temperatures for 8788 atoms specimen.

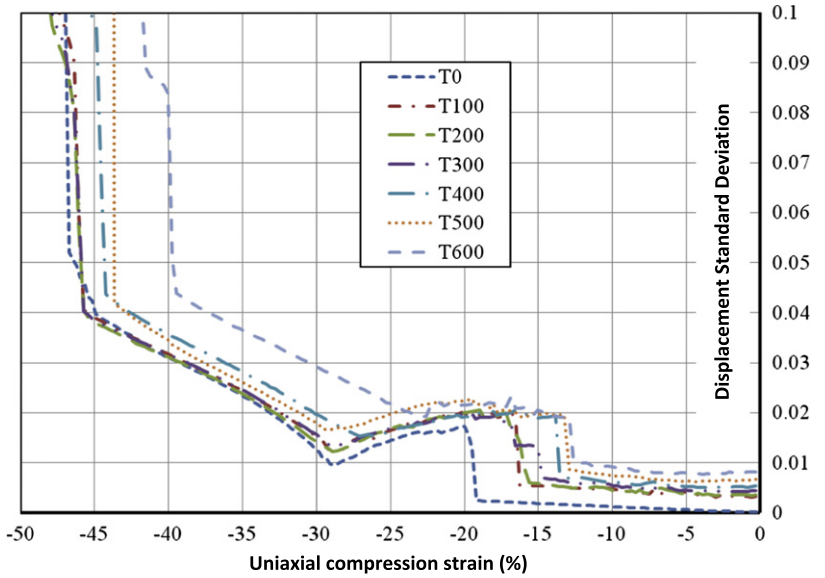

Fig. 10. Uniaxial deformation; the evolution of DSD versus uniaxial compression strain at various temperatures for 8788 atoms specimen.

The time step of MD simulations is set to 0.001 dimensionless time, as a micro-time step. The specimens were simulated on 0, 100, 200, 300, 400, 500, 600 and 700 °K. At higher temperatures, it has been observed that the corners of crystalline lattice are deformed and become curved. At temperatures larger than 900 °K, the solid to fluid transition has been obvious. The occurrence of this phase transition can be confirmed by the fact that the Gold cube becomes liquid at 1337 °K, in which there is no pressure on the surface of specimens. In modeling of temperature, the specimens are relaxed to achieve a specific temperature, and obtain the stability condition for the size of cube. This procedure is performed by the proper relaxation rate to forbid the structure instability and atom departure. In Table 1, the effect of total simulation time and the number of time steps on the stability of system are given for 4000 atoms specimen at 400 °K. As can be seen from this table, the size of cube has been fixed at three directions and specimens become stable by increasing the total simulation time.

In Fig. 1, the variation of temperature is plotted with micro-time steps after relaxation phase for 4000 atoms specimen at 500 °K. The average micro-time steps are accomplished by 80,000 steps per 100 °K and the total simulation time sets to 40 picoseconds per 100 °K. After relaxation phase, two planes of boundary atoms at each side of cube are fixed on their relaxed lattice site. The cut-off radius is the radius at which atoms are restricted at all temperatures and forbids the inner atom to exit from the structure walls. The number of restricted atoms is assumed to be constant at all temperatures in each specimen, and the rate of deformation is assumed to be constant with 10^6 micro-time steps per 20% strain. The displacement-control algorithm is employed in all simulations. The boundary displacement in MD simulation is identical to CB deformation, and is divided into 100 identical macro-time steps per 10% strain, in which each portion of deformation is implemented at the first micro-time step of each macro-time step. All boundary atoms are subjected to this portion of

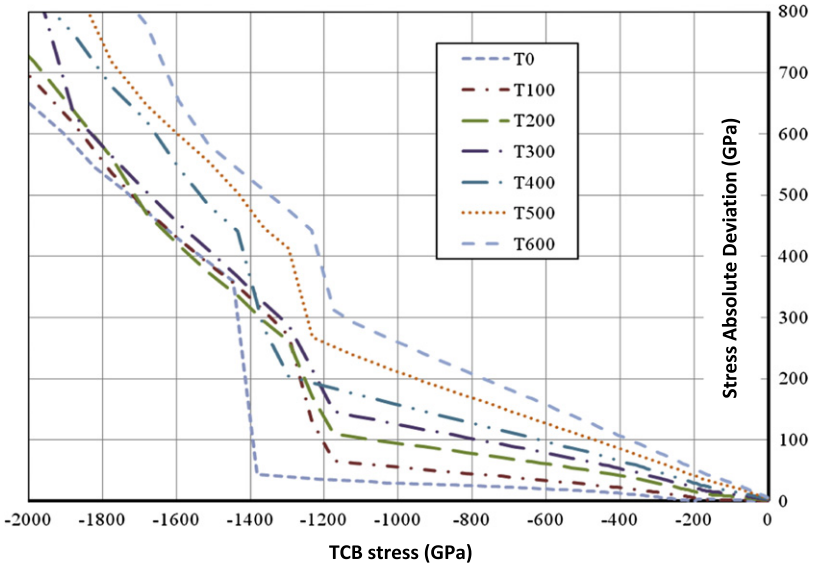

Fig. 11. Uniaxial deformation; the evolution of SAD versus TCB compression stress at various temperatures for 8788 atoms specimen.

deformation during the macro-time step. The remaining atoms are released to reach a position which locally minimizes the total potential energy of the system. The Nose–Hoover thermostat is employed to control the temperature of specimen. The thermostat parameter Q depends on the size of sample, and is obtained at each position to restrain the temperature. The results of DSD and SAD are calculated at the last micro-step of each macro-time step. In order to verify the validity of results derived by the proposed MD model, the lattice parameter is obtained for Nickel with 1372 atoms specimen at various temperatures. The results obtained by present model are in complete agreement with those reported by Dupuy et al. [23], as shown in Fig. 2.

4.1. Simple shear deformation

The deformation gradient tensor for the simple shear deformation can be given by

$$\mathbf{F} = \begin{bmatrix} 1 & \tan\theta & 0 \\ 0 & 1 & 0 \\ 0 & 0 & 1 \end{bmatrix} = \begin{bmatrix} 1 & \alpha & 0 \\ 0 & 1 & 0 \\ 0 & 0 & 1 \end{bmatrix}$$

where α and θ are the shear number and shear angle respectively. All four specimens are subjected to the simple shear deformation for the temperature range from 0 to 700 °K. The ultimate shear strain is set to 23%. The break point of TCB hypothesis is defined by the point that dislocations are observed in the sample and therefore the values of DSD and SAD increases intensively.

In Figs. 3 and 4, the behavior of 4000 atoms specimen are shown at 100 °K and 500 °K. In these figures, the initiation of dislocation is shown together with the behavior of specimen and its break point. The trend of DSD versus shear strain is similar at both temperatures, however, the dislocation is initiated earlier in the temperature of 500 °K at the shear strain of 13.21%. In Fig. 5, the variations of SAD shear stress are plotted with the TCB shear stress at various temperatures. Obviously, the breakpoint of SAD diagram decreases by increasing the temperature. This figure presents that higher temperatures have higher stress deviations for the TCB stress less than 11.5 GPa. As a result the specimen with higher temperature has broken down earlier, and the breakpoint of stress deviation reduces by increasing the temperature. In Fig. 6, the evolutions of DSD value versus shear number are depicted at different temperatures. This figure illustrates that by increasing the temperature, the breakpoint of DSD diagram occurs at lower shear strain. Furthermore, it can be observed that the value of DSD value increases by increasing the temperature at the same shear number for the strain between 0 and 12%. In Fig. 7, the variations of BDT shear stress with shear strain are plotted at various temperatures. Obviously, the BDT shear stress decreases by increasing the temperature.

4.2. Uniaxial tension and compression deformations

In 3D continuum mechanics, the uniform uniaxial deformation gradient **F** applied to the system can be defined as

$$\mathbf{F} = \begin{bmatrix} \partial x/\partial X & 0 & 0 \\ 0 & 1 & 0 \\ 0 & 0 & 1 \end{bmatrix} = \begin{bmatrix} \lambda & 0 & 0 \\ 0 & 1 & 0 \\ 0 & 0 & 1 \end{bmatrix}$$

where $\lambda - 1$ is the uniaxial strain which is equal to the magnitude of the uniaxial deformation divided by the initial length of the specimen. If $\lambda > 1$, it exhibits the tensile strain and if $\lambda < 1$, it is the compressive strain. In order to investigate the effect of temperature and its correlation with the size of specimen, the samples with different sizes and various temperatures are subjected to tension and compression deformations. In Fig. 8, the variations of DSD with uniaxial strain are plotted for 8788 atoms specimen at different temperatures. As can be seen from this figure, the temperature has a significant effect on the strain deviation, in which the tension specimen with higher temperature has greater strain deviation and lower failure point. The evolutions of SAD versus uniaxial tension strain are plotted in Fig. 9 for different temperatures. Obviously, for the uniaxial tension strain less than 6%, the stress deviation of tensile sample increases by increasing the temperature. It is worth mentioning that all simulations are carried out here based on the displacement-control manner. In fact, the prescribed displacement imposed on the boundaries of specimen prevents the violation of atoms by restraining the boundary atoms. Hence, the displacements obtained by the MD model are more verifiable at high temperatures and the trend of DSD versus tensile strain cannot be affected by the temperature. As presented earlier, the BDT stress obtained by the MD simulations is proportional to the second order of distance of inner atoms and their neighbors, while the displacement of MD structure

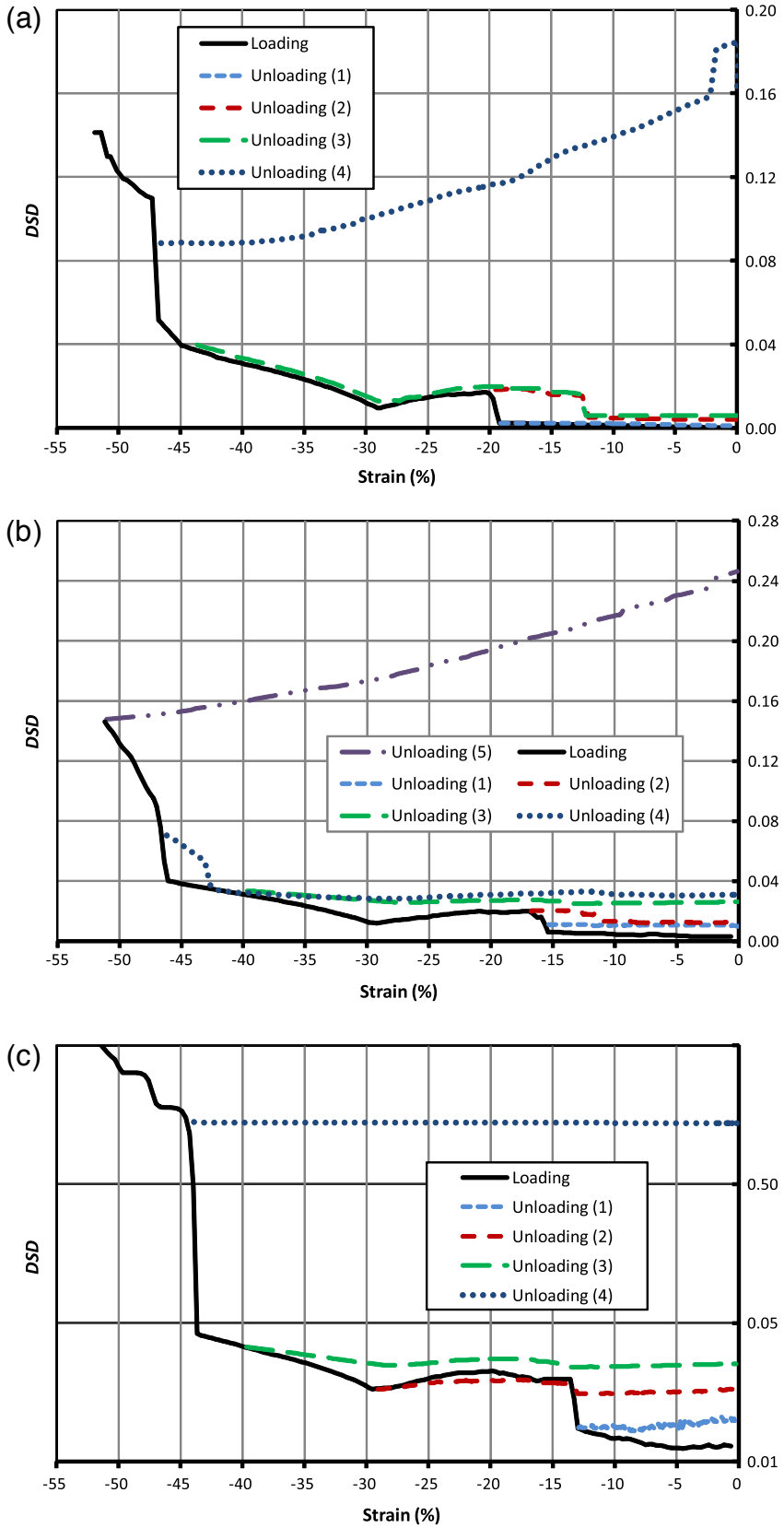

Fig. 12. The variations of DSD with the compressive strain for unloading process of 8788 atom specimens at; (a) $T = 0°$, (b) $T = 100°$ and (c) $T = 500$ °K. The specimens are unloaded from four levels. The first and second levels are before and after the first break point of temperature-related CB hypothesis, respectively. The third and forth levels are before and after the third break point of TCB hypothesis, respectively.

is proportional to first order. Thus, the values of stresses increase considerably in MD model at higher temperatures. Furthermore, at higher temperatures, atoms display high vibrational frequency, in which by imposing the deformation on atomic structure, the

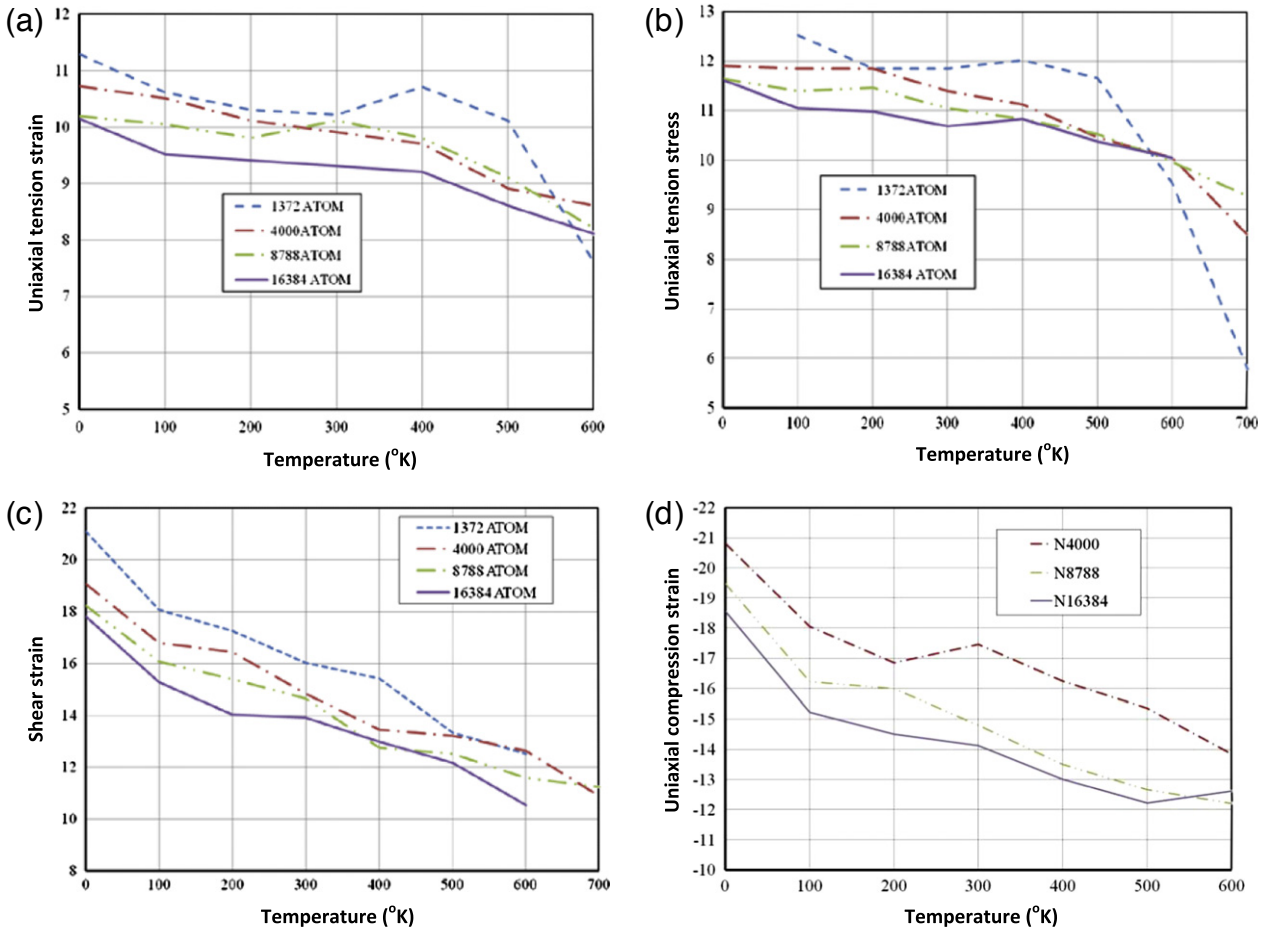

Fig. 13. The variations with temperature of: (a) the uniaxial tension strain, (b) the uniaxial tension stress, (c) the shear strain, (d) the uniaxial compression strain at the break points for various specimens.

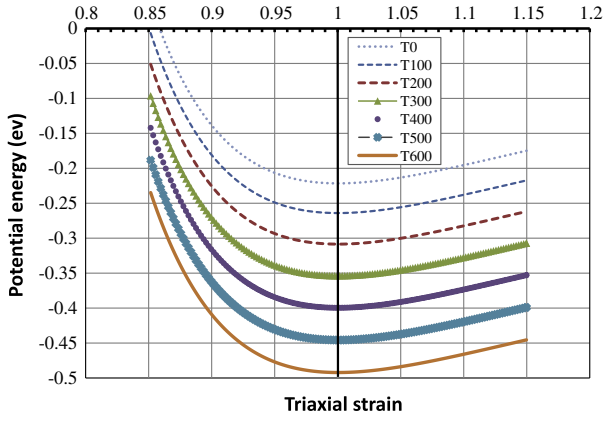

Fig. 14. The potential energy versus triaxial strain for 3D Gold bulk at various temperatures.

vibrational frequency is moderated and the variation of average stress is diminished. On the other hand, in the temperature-related CB rule, the stress decreases by increasing the temperature due to the volumetric growth, and as a result, the stress absolute deviation decreases by increasing the uniaxial strain up to the break point of 6%, as shown in Fig. 9. However, the SAD value decreases by increasing the uniaxial tension strain to the point that the stress deviation takes the minimum value. This value reduces by increasing the temperature, and the slope of SAD graph decreases. It can be concluded that the breakpoint of stress deviation decreases by increasing the temperature in tension.

The compressive samples demonstrate complex behavior with the temperature, as it was also reported by Aghaei et al. [11] at zero temperature. In Fig. 10, the evolutions of DSD versus uniaxial compression strain are plotted for various temperatures. Clearly, three distinct break points can be observed in the strain field. At the first breakpoint of DSD diagram, the strain deviation is about 0.002 to 0.01. If this discrepancy is assumed as the failure criterion, the TCB hypothesis fails at the first breakpoint of DSD diagram, as shown in Fig. 10. It can be observed that the specimen with higher temperature has greater strain deviation; the first breakpoint of DSD diagram happens earlier, and the TCB hypothesis fails at lower strain. It was reported by Khoei et al. [10] that the first and second breakpoints present the elastic material behavior, however – the third breakpoint expresses the plastic behavior, in which the specimen dose not return to its initial position in unloading process. In addition, the strain deviation of third breakpoint increases severely, which can be considered as the failure point for TCB hypothesis. In Fig. 11, the evolutions of SAD versus TCB compression stress are plotted for different temperatures. Comparing the results of tension and compression specimens, it can be deduced that the material is more stable and the TCB hypothesis is more valid at lower temperatures, as shown in Fig. 11.

In order to investigate the effect of temperature on material yield point, the specimens are unloaded from various distinct points at 0, 100 and 500 °K, as shown in Fig. 12. To maintain the temperature of the system constantly, all MD simulations are per-

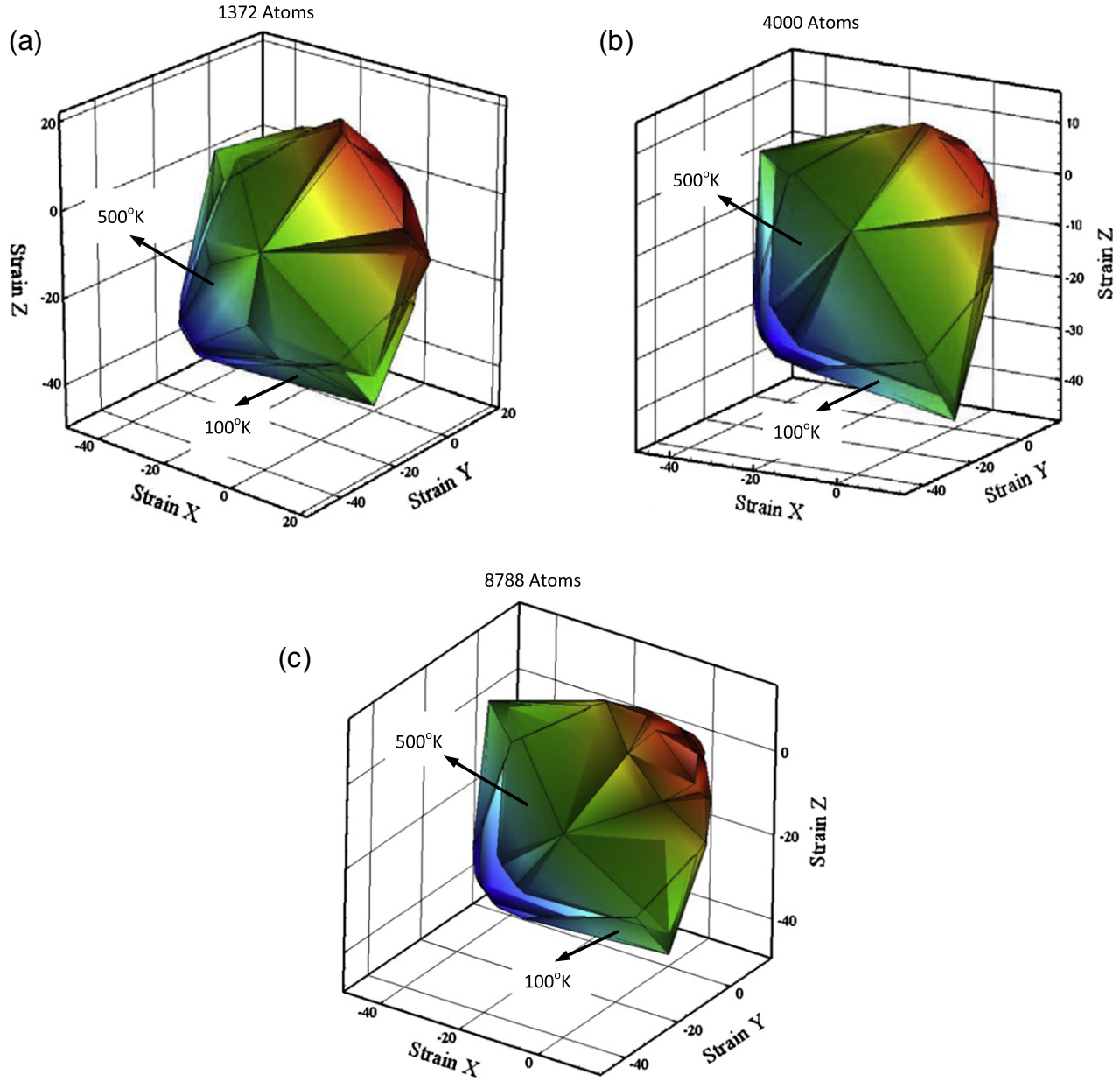

Fig. 15. The validity surfaces for (a) 1372, (b) 4000, and (c) 8788 atoms specimens; the inner surface belongs to 500 °K and the outer surface belongs to 100 °K temperature.

formed in NVT ensemble and the Nose–Hoover thermostat is utilized to control the temperature. Note that if the velocity of particles is reversed, it is not necessary to return to the initial configuration of the system. Moreover by implementing the effect of temperature in atomic structure, atoms experience more disturbances at higher temperatures. As shown in Fig. 12b and c, the atomic structure cannot return to its initial configuration precisely in unloading process at the temperatures of 100 and 500 °K. In fact, the *DSD* value of unloading process is not exactly compatible with its loading value after the first break point at higher temperatures, in which this inconsistency intensifies by increasing the temperature. Furthermore, the atomic structure experiences some large deformations from initial configuration and more intense disturbance in plastic deformation at higher temperatures. In spite of this fact, the DSD value of unloading process at zero temperature is well-matched with the loading process, as shown in Fig. 12a.

In order to investigate the size effect of specimens, the samples with different sizes are subjected to tension and compression deformation paths at different temperatures. In Fig. 13, the variations with temperature of the uniaxial tension strain, the uniaxial tension stress, and the shear strain are plotted at the break points for various specimens, including 1372, 4000, 8788 and 16,384 atoms. The temperature effect in various specimens shows that larger samples in tensile deformation have a smoother behavior. However, the material is stable for both strain and stress domains at various temperatures, and the TCB is valid in compression rather than tension.

4.3. Triaxial tests and validity surface

In order to illustrate the stability of atomic structure in minimum potential energy, the variations of potential energy are plotted with triaxial strain for 3D Gold bulk at various temperatures in Fig. 14. It must be noted that in undeformed configuration, the lattice must not experience any kind of stress and the potential energy of the system should be minimal. However, due to the degeneracy of initial configuration of atoms, the lattice must be de-

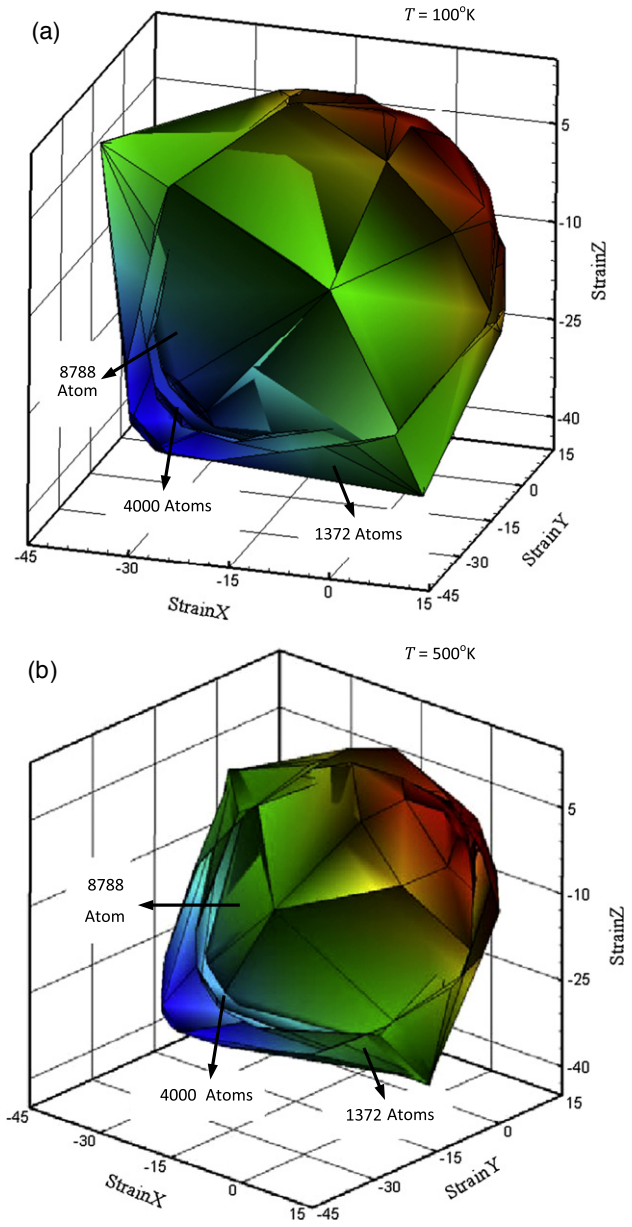

Fig. 16. The validity surfaces for 1372, 4000 and 8788 atom specimens at; (a) temperature 100 °K, (b) temperature 500 °K (the inner surface belongs to the larger specimen and outer layer belongs to the smaller specimen).

formed to release its residual stress. This phenomenon is called as the relaxation procedure in molecular dynamics simulations. Fig. 14 presents the configuration that locally minimizes the potential energy of the system and the atoms are in their stable states. Obviously, the system has different minimal points for different temperatures. Due to the fact that atoms with higher temperature vibrate in higher speed, the system experiences more situations in the phase space, and the minimum potential energy of the system decreases.

In order to investigate the temperature effects on validity surface of Cauchy–Born hypothesis, three specimens with 1372, 4000 and 8788 atoms are subjected to various combinations of strains in x, y and z-directions at two temperatures of 100 and 500°K. According to DSD and SAD diagrams and the stress–strain curves of each simulation, the first breakpoint of each specimen is determined. On the virtue of symmetry of cubic specimens, each break point represents six points in three-dimensional space. In Fig. 15, the validity surfaces are depicted in strain space for three specimens at temperatures 100 and 500 °K. The validity surface is a simply-connected and convex surface, in which the TCB hypothesis is valid and the material is elastic inside the surface. The TCB is invalid outside the surface and the crystalline material can experience either elastic or plastic deformation. Fig. 15 indicates that the validity surfaces become smaller at higher temperature, which is significant in larger specimen. In Fig. 16, the validity surfaces are represented at temperatures of 100 and 500 °K for 1372, 4000 and 8788 atom specimens. As can be observed, the size effect is more considerable at higher temperatures and the larger specimens yield more quickly than small specimens at higher temperatures, which uphold the same consequence reported by Aghaei et al. [11] at zero temperature.

5. Conclusion

In the present paper, the temperature effects and the validity of temperature-related Cauchy–Born hypothesis were presented in three-dimensional lattice structures by comparatively analyzing results of the continuum mechanics calculation and molecular dynamics simulations. Three-dimensional temperature-related Cauchy–Born equations were developed and the stability and size-dependency of temperature-related Cauchy–Born hypothesis were investigated by means of direct comparison between atomistic and continuous mediums information. In MD simulations, the Sutton–Chen many-body potential was employed, and the Nose–Hoover thermostat was applied to control the temperature. The temperature control in MD simulation was performed at constant temperature rather than the constant energy.

The trend of DSD diagram with shear strain highlighted that the dislocation is initiated earlier at higher temperature. Also, the breakpoint of SAD diagram and the BDT shear stress decrease by increasing the temperature. In addition, the tension specimen with higher temperature has greater strain deviation and lower failure point. It was observed from the compressive samples that the specimen with higher temperature has greater strain deviation; the first breakpoint of DSD diagram happens earlier, and the TCB hypothesis fails at lower strain. It was pointed out that the material is more stable and the TCB hypothesis is more valid at lower temperatures. It is shown that the validity surfaces become smaller at higher temperature, which is significant in larger specimen. It has been concluded that in temperature-related CB model, the resultant curves illustrate a strong correlation between the material stability and thermal conditions.

Acknowledgement

The authors are grateful for the research support of the Iran National Science Foundation (INSF).

References

[1] J. Wang, S. Yip, S. Phillpot, D. Wolf, Phys. Rev. Lett. 71 (1993) 4182–4185.
[2] A. Braides, G. Dal Maso, A. Ggarroni, Arch. Rat. Mech. Anal. 146 (1999) 23–58.
[3] P.A. Klein, H. Gao, Eng. Fract. Mech. 61 (1998) 21–48.
[4] P. Zhang, Y. Huang, H. Gao, K.C. Hwang, Int. J. Solids Struct. 39 (2002) 3893–3906.
[5] G. Friesecke, F. Theil, J. Nonlinear. Sci. 12 (2002) 445–478.
[6] G. Friesecke, R.D. James, J. Mech. Phys. Solids 48 (2000) 1519–1540.
[7] M. Arroyo, T. Belytschko, J. Mech. Phys. Solids 50 (2002) 1941–1977.
[8] P. Zhang, P. Klein, Y. Huang, H. Gao, P.D. Wu, Comput. Modell. Eng. Sci. 3 (2002) 263–277.
[9] H. Jiang, P. Zhang, B. Liu, Y. Huang, P.H. Geubelle, K.C. Hwang, Comput. Mater. Sci. 28 (2003) 429–442.
[10] A.R. Khoei, M.J. Abdolhosseini Qomi, M.T. Kazemi, A. Aghaei, Comput. Mater. Sci. 44 (2009) 999–1006.
[11] A. Aghaei, M.T. Kazemi, M.J. Abdolhosseini Qomi, A.R. Khoei, Int. J. Solids Struct. 46 (2009) 1925–1936.

[12] M.J. Abdolhosseini Qomi, A. Aghaei, A.R. Khoei, Int. J. Numer. Methods Eng., in press. doi:10.1002/nme.2995.
[13] H. Jiang, Y. Huang, K.C. Hwang, ASME J. Eng. Mater. Technol. 127 (2005) 408–416.
[14] D.W. Brenner, Phys. Rev. 42 (1990) 9458–9471.
[15] S. Xiao, W. Yang, Comput. Mater. Sci. 37 (2005) 374–379.
[16] G. Yun, H.S. Park, Comput. Methods Appl. Mech. Eng. 197 (2008) 3337–3350.
[17] W. Yang, S. Xiao, Comput. Mater. Sci. 41 (2007) 431–439.
[18] J.M. Rickman, R. LeSar, Ann. Rev. Mater. Res. 32 (2002) 195–217.
[19] A.P. Sutton, J. Chen, Philos. Mag. 61 (1990) 139–146.
[20] M.P. Allen, D.J. Tildesley, Computer Simulation of Liquids, Clarendon Press, Oxford, 1987.
[21] G.J. Martyna, M.L. Klein, J. Chem. Phys. 97 (1992) 2635–2643.
[22] A.K. Subramanian, C.T. Sun, Int. J. Solids Struct. 45 (2008) 4340–4346.
[23] L. Dupuy, E.B. Tadmor, R.E. Miller, R. Phillips, Phys. Rev. Lett. 95 (2005) 060202.